processes MDPI

Article

A Dynamic Partition Model for Multi-Energy Power Grid Energy Balance Considering Electric Vehicle Response Willingness

Shi Qiu [1], Kun Zhang [1,*], Zhuo Chen [1], Yiling Ma [2] and Zhe Chen [1,3]

[1] Shenyang University of Technology, Shenyang 110870, China
[2] Electric Power Research Institute of State Grid Liaoning Electric Power Co., Ltd., Shenyang 110055, China
[3] Aalborg University, 9220 Aalborg, Denmark
* Correspondence: zhangkun@sut.edu.cn

Abstract: In multi-energy power grids in which electric vehicles (EVs) participate in response, there are significant differences in the power balance between multi-energy supply and load at different time scales and spatial scales. To optimize the energy balance demand of each region, this paper proposes a dynamic partition coordination model for power grid energy regulation demand that considers the willingness of electric vehicles to respond and the uncertainties related to sources, loads, and storage. Firstly, the charging and discharging characteristics of multi-energy conversion devices in power grids, as well as the response uncertainties of these devices, are studied, and a source, load, and storage uncertainty model is established. Then, based on the Markov random field theory and the energy prior model, the dynamic partition model and its solution algorithm for the multi-energy power grid are proposed. Finally, a simulation system is established based on the actual operating data of a multi-energy power grid, and the proposed method is simulated and analyzed. The results indicate that the energy balance partition optimization method proposed in this article is effective. The application of the method proposed in this article can fully leverage the regulatory potential of energy conversion equipment, effectively reduce the proportion of traditional energy supply and peak shaving capacity, and improve the utilization rate of renewable energy.

Keywords: multi-energy power grid; energy balance; power grid partition; multi-energy storage; electric vehicle response

check for updates

Citation: Qiu, S.; Zhang, K.; Chen, Z.; Ma, Y.; Chen, Z. A Dynamic Partition Model for Multi-Energy Power Grid Energy Balance Considering Electric Vehicle Response Willingness. *Processes* **2023**, *11*, 1508. https://doi.org/10.3390/pr11051508

Academic Editors: Qiuye Sun, Rui Wang and Zhengmao Li

Received: 10 April 2023
Revised: 10 May 2023
Accepted: 12 May 2023
Published: 15 May 2023

Correction Statement: This article has been republished with a minor change. The change does not affect the scientific content of the article and further details are available within the backmatter of the website version of this article.

1. Introduction

With the development and utilization of new energy, the large-scale grid connection of new energy has brought many challenges to the smooth and efficient operation of traditional power grids, among which the energy exchange and balance issues between regional interconnected systems of multiple energy grids are noteworthy [1,2]. When the energy balance adjustment of a multi-energy grid is required at various time scales, the energy imbalance often starts from a certain node or a local area of the multi-energy grid. In most cases, it is neither necessary nor advisable to adjust the energy balance from the overall perspective of the multi-energy grid network, and doing so may even lead to an increase in network loss. Instead, according to the peak shaving demand of the multi-energy grid in different peak shaving capacities and different energy forms, realizing the peak shaving optimization of different energy forms of multi-energy grid will lead to quickly and accurately judge the local areas or nodes with energy imbalances and the energy forms of energy regulation demand of the multi-energy grid [3–6].

At present, domestic and foreign scholars have carried out a lot of research on the energy regulation demand of multi-energy grids. Reference [7] proposed a multi-energy participant (MEP) behavior prediction model based on signal price coupling that optimizes the energy balance of multi-energy systems based on signal price. An energy control method based on a multi-energy energy storage system was proposed in [8] to optimize power grids in consideration of economy and stability. The modified prediction percentage of dissatisfaction (PPD) index, related to thermal environment parameters, was introduced in [9] to realize a comprehensive evaluation of energy storage. Different power grid optimization methods were analyzed in [10], considering the accuracy, complexity, and stability of the studied models, and a dynamic optimal energy flow model was established based on the multi-objective optimization method. Reference [11] mainly studied the frequency regulation and carbon emission reduction regulation capabilities of multi-energy storage devices in power systems.

In [12], a new flexible supply-demand balance analysis system for multi-energy systems was proposed considering the spatial correlation modeling and time sequence connection of component states. Reference [13] proposed an economic dispatch model for multi-energy systems based on marginal prices that enhanced the multi-energy complementary regulation capability of multi-energy systems by reducing the regulation cost of multi-energy units.

EVs can play a flexible regulatory role in the power system with their schedulable potential [14]. Reference [15] considered charging uncertainty and energy satisfaction while modeling EVs, and took EVs to be the main flexible resources to participate in the economic dispatch of the power system. However, under that study's scheduling architecture, the power system dispatch center needed to process a large amount of EV user data and perform power system optimization scheduling, resulting in complex and heavy computational tasks. Considering the small battery capacity and low charging and discharging power of a single EV, the data volume of EV users is large. Reference [16] proposed a charging-station-based electric vehicle scheduling strategy based on game theory. In the proposed strategy, the charging time of electric vehicles was planned with the goal of minimizing the imbalance between supply and demand in the power grid.

At present, the literature provides some theoretical support for energy regulation in multi-energy grids, but it has not fully considered the response willingness and uncertainty of electric vehicles [17] and the dynamic zoning coordination of multi-energy grids. There is still great room for improvement in optimizing the coordination of energy regulation demand in multi-energy grids [18].

This article proposes a dynamic zoning coordination model for energy regulation demand in multi-energy grids, taking into account the willingness of electric vehicles to respond and the uncertainty of grid source, load, and storage. Firstly, considering the uncertainty of electric vehicle response willingness and new energy sources, loads, and multi-energy storage, a source load storage uncertainty model is established. Then, the energy balance correlation between the adjacent nodes of a multi-energy power system network is measured according to the characteristic index of multi-energy balance correlation measurement, and a regional division model of multi-energy balance based on a high-order Markov random field of multi-energy balance correlation is established. Then, by studying the high-order topological structure prior model and Markov random field model of multi-energy balance characteristics, the dynamic division model of multi-energy balance area and its solution algorithm are proposed. Finally, the effectiveness of the proposed model in this paper is verified by constructing a simulation of multi-energy balance zoning characteristics and optimizing the energy regulation demand of multi-energy power systems.

2. Source, Load, and Storage Uncertainty Model

2.1. Uncertainty Model of Electric Vehicles

(1) EV Energy Boundary Model

The feasible range of charging and discharging for EVs can be described by their energy and power boundaries, that is $\left\{e_i^{+/(-)}(t), p_i^{+/(-)}(t)\right\}$, the feasible set representing all possible charge and discharge trajectories. The corresponding electricity and power boundaries are represented as follows:

$$e_i(t) = e_i^{\mathrm{s}} + \int_{t_i^{\mathrm{s}}}^{t} p_i(t)\mathrm{d}t = Q_i S_i^{\mathrm{s}} + \int_{t_i^{\xi}}^{t} p_i(t)\mathrm{d}t \tag{1}$$

$$e_i^{+}(t) = \begin{cases} \min\left(e_i(t-\Delta t) + p_i^{\mathrm{c}}\eta_{\mathrm{c}}\Delta t, e_i^{\max}\right) & t \in \left[t_i^{\mathrm{s}}, t_i^{\mathrm{d}}\right] \\ 0 & t \notin \left[t_i^{\mathrm{s}}, t_i^{\mathrm{d}}\right] \end{cases} \tag{2}$$

$$e_i^{-}(t) = \begin{cases} \max\left(e_i(t-\Delta t) + p_i^{\mathrm{d}}\Delta t/\eta_{\mathrm{d}}, e_i^{\min}, \quad e_i^{\mathrm{d}} - p_i^{\mathrm{c}}\eta_{\mathrm{c}}\left(t_i^{\mathrm{d}} - t\right)\right) & \\ 0 & t \in \left[t_i^{\mathrm{s}}, t_i^{\mathrm{d}}\right] \\ 0 & t \notin \left[t_i^{\mathrm{s}}, t_i^{\mathrm{d}}\right] \end{cases} \tag{3}$$

$$p_i^{+}(t) = \begin{cases} p_i^{\mathrm{c}}\eta_{\mathrm{c}} & t \in \left[t_i^{\mathrm{s}}, t_i^{\mathrm{d}}\right] \\ 0 & t \notin \left[t_i^{\mathrm{s}}, t_i^{\mathrm{d}}\right] \end{cases} \tag{4}$$

$$p_i^{-}(t) = \begin{cases} \frac{p_i^{\mathrm{d}}}{\eta_{\mathrm{d}}} & t \in \left[t_i^{\mathrm{s}}, t_i^{\mathrm{d}}\right] \\ 0 & t \notin \left[t_i^{\mathrm{s}}, t_i^{\mathrm{d}}\right] \end{cases} \tag{5}$$

where i is the sequential number of the electric vehicle, $e_i(t)$ and $p_i(t)$ are the electric quantity and power of the EV at time t, respectively, e_i^{s} is the initial battery level when the EV is connected to the network, e_i^{d} is the battery level when the EV is off the grid, Q_i and S_i^{s} are the rated capacity and initial SOC of the EV, respectively, $e_i^{+/(-)}(t)$ and $p_i^{+/(-)}(t)$ are the upper and lower boundaries of the electric quantity and power of the EV at time t, t_i^{s} and t_i^{d} are the times when EV enters and leaves the network, respectively, $e_i^{\max}$ is the maximum value of EV power, $e_i^{\min}$ is the minimum threshold of battery capacity to prevent the excessive discharge of the EV, p_i^{c} and p_i^{d} are the rated charging power and discharge power of the EV, and η_{c} and η_d are the charging efficiency and discharge efficiency of the EV.

(2) Uncertainty Model of Electric Vehicle Response

In practice, the uncertainty of EV users' response behavior is caused by factors such as travel habits and sensitivity to incentive levels [19]. Taking into account this uncertainty, the schematic diagram of EV users' willingness to respond is shown in Figure 1. The black solid line in the figure represents the EV user response willingness curve based on consumer psychology principles, and the area in the figure can be divided into the dead zone, linear zone, and saturation zone as the incentive price changes. The red dashed line represents the maximum fluctuation curve of EV response willingness.

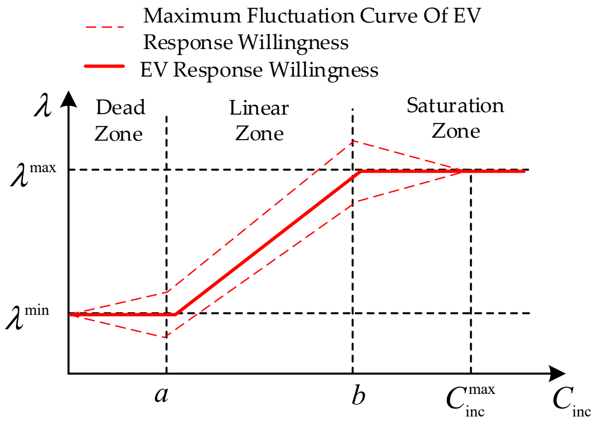

Figure 1. Schematic diagram of the uncertainty in EV user response intention.

From Figure 1, it can be seen that in the dead zone and linear zone, when the incentive level is not high enough, the response uncertainty mainly depends on non-economic factors. EV users' willingness to respond increases with an increase in incentive prices, and the response uncertainty also increases in this situation. In the saturation zone, the incentive level is sufficiently attractive to users, and the response uncertainty is mainly determined by economic factors. As the incentive level increases, the response willingness has reached its upper limit, but the response uncertainty gradually decreases to zero.

EV users' willingness to respond and response bias are calculated thus:

$$\lambda(C_{\text{inc}}) = \begin{cases} 0 \pm d_\lambda & 0 \leqslant C_{\text{inc}} \leqslant a \\ k(C_{\text{inc}} - a) \pm d_\lambda & a < C_{\text{inc}} \leqslant b \\ \lambda^{\max} \pm d_\lambda & b < C_{\text{inc}} \leqslant C_{\text{inc}}^{\max} \\ \lambda^{\max} & C_{\text{inc}} > C_{\text{inc}}^{\max} \end{cases} \tag{6}$$

$$d_\lambda = \begin{cases} k_1 C_{\text{inc}} & 0 \leqslant C_{\text{inc}} \leqslant b \\ k_1 b + k_2(C_{\text{inc}} - b) & b < C_{\text{inc}} \leqslant C_{\text{inc}}^{\max} \\ 0 & C_{\text{inc}} > C_{\text{inc}}^{\max} \end{cases} \tag{7}$$

Here, $\lambda(C_{\text{inc}})$ is the willingness of EV users to respond under incentive compensation C_{inc}, and $\lambda(C_{\text{inc}}) \in [0, 1]$. The larger the value of $\lambda(C_{\text{inc}})$ is, the stronger the user's willingness to respond becomes. d_λ is the maximum fluctuation range in response to willingness, a and b are the excitation levels for the dead zone inflection points and saturation zone inflection points, respectively, $C_{\text{inc}}^{\max}$ is the upper limit of the incentive level, $\lambda^{\max}$ and $\lambda^{\min}$ are the maximum and minimum response willingness coefficients of users, respectively, and k, k_1, and k_2 are constant coefficients.

2.2. Energy Uncertainty Model for Renewable Energy Sources

(1) Energy Uncertainty Model of Wind Power Supply

Assuming that the uncertainty of energy output for each wind farm station in the multi-energy grid follows a normal distribution [20], the wind power energy output characteristics considering uncertainty can be expressed thus:

$$X_{wPO}(t) = \begin{cases} \int_{t-\Delta t}^{t} [P_{WPO\eta}(t) \pm \Delta\varepsilon_{WP\eta}] dt, \forall t \in [t_{vr}, t_{vc}] \\ \int_{t-\Delta t}^{t} [P_{WPO_r}(t) \pm \Delta\varepsilon_{WPr}] dt, \forall t \in [t_{vi}, t_{vr}] \\ 0, \forall t \in [t_{v0}, t_{vi}] \end{cases} \tag{8}$$

where X_{wPO} is the energy output of the wind power generation system within a time interval Δt, $P_{WPO\eta}$ is the wind power output under the condition that the wind speed in the wind farm is higher than the inlet wind speed and lower than the rated wind speed, P_{WPO_r} is the wind power output when the wind speed in the wind farm is higher than the rated wind speed and lower than the cutout wind speed, $\Delta\varepsilon_{WP\eta}$ is the uncertainty of wind power output when the wind speed inside the wind farm is higher than the wind speed inside the wind farm and lower than the rated wind speed, $\Delta\varepsilon_{WPr}$ is the uncertainty of wind power output when the wind speed in the wind farm is higher than the rated wind speed and lower than the cutout wind speed, t_{vi} is the moment when the wind speed in the wind farm is higher than the start of the wind speed, t_{vr} is the moment when the wind speed in the wind farm is higher than the start time of the rated wind speed, and t_{vc} is the moment when the wind speed in the electric field is higher than the start time of the cutting wind speed.

The probability distribution function of the wind power output uncertainties $\Delta\varepsilon_{WP\eta}$ and $\Delta\varepsilon_{WPr}$ can be expressed thus:

$$\begin{cases} f_{WP}(\Delta\varepsilon_{WP\eta}) = \frac{1}{\sqrt{2\pi}\sigma_{WP\eta}} \exp\left(-\frac{\Delta\varepsilon_{WP\eta}^2}{2\sigma_{WP\eta}}\right) \\ f_{WP}(\Delta\varepsilon_{WPr}) = \frac{1}{\sqrt{2\pi}\sigma_{WPr}} \exp\left(-\frac{\Delta\varepsilon_{WPr}^2}{2\sigma_{WPr}}\right) \end{cases} \tag{9}$$

where $\sigma_{WP\eta}$ and σ_{WPr} represent the maximum uncertainties of wind power output under different wind speed conditions.

(2) Energy Uncertainty Model of Photovoltaic Power Supply

It is assumed that the uncertainty of energy output for photovoltaic power stations in the multi-energy grid follows normal distribution at time intervals Δt. Then, the photovoltaic energy output characteristics considering uncertainty can be expressed thus:

$$X_{PVO}(t) = \begin{cases} \int_{t-\Delta t}^{t} \left[P_{PVO\eta}(t) \pm \Delta\varepsilon_{PV\eta}\right] dt, \forall t \in \left[t_{\varphi i}, t_{\varphi r}\right] \\ \int_{t-\Delta t}^{t} \left[P_{PVOr}(t) \pm \Delta\varepsilon_{PVr}\right] dt, \forall t \in \left[t_{\varphi r}, t_{\varphi c}\right] \\ 0, \qquad \forall t \in \left[t_{\varphi 0}, t_{\varphi i}\right] \end{cases} \tag{10}$$

where X_{PVO} is the energy output of photovoltaic power generation system over time intervals Δt, $P_{PVO\eta}$ is the photovoltaic output power when the solar radiation intensity in the photovoltaic power station is higher than the minimum intensity and lower than the rated intensity, P_{PVOr} is the photovoltaic output power when the solar radiation intensity in the photovoltaic power station is higher than the rated intensity, $\Delta\varepsilon_{PV\eta}$ is the uncertainty of photovoltaic power output when the solar radiation intensity in a photovoltaic power station is higher than the minimum required intensity and lower than the rated intensity, $\Delta\varepsilon_{PVr}$ is the uncertainty of photovoltaic power output when the solar radiation intensity of photovoltaic power station is higher than the rated intensity, $t_{\varphi i}$ is the starting time when the solar radiation intensity in the photovoltaic power station is higher than the minimum required intensity, $t_{\varphi r}$ is the moment when the solar radiation intensity in the photovoltaic power station is higher than the initial rated intensity, $t_{\varphi c}$ is when the solar radiation intensity in the photovoltaic power station is higher than the end of the rated intensity, and $t_{\varphi 0}$ is the starting time when the solar radiation intensity in the photovoltaic power station is lower than the minimum required intensity.

The probability distribution function of the energy output uncertainties of the photovoltaic power generation system,$\Delta\varepsilon_{PV\eta}$ and $\Delta\varepsilon_{PVr}$, can be expressed thus:

$$\begin{cases} f_{PV}(\Delta\varepsilon_{PV\eta}) = \frac{1}{\sqrt{2\pi}\sigma_{PV\eta}} \exp\left(-\frac{\Delta\varepsilon_{PV\eta}^2}{2\sigma_{PV\eta}}\right) \\ f_{PV}(\Delta\varepsilon_{PVr}) = \frac{1}{\sqrt{2\pi}\sigma_{PVr}} \exp\left(-\frac{\Delta\varepsilon_{PVr}^2}{2\sigma_{PVr}}\right) \end{cases} \tag{11}$$

where $\sigma_{PV\eta}$ and σ_{PVr} represent the maximum uncertainty of photovoltaic power generation system output under different conditions of solar radiation intensity.

2.3. Load Uncertainty Model

Assuming that the load power consumption uncertainty follows normal distribution in time intervals [21], the energy property considering uncertainty can be expressed thus:

$$X_{UCL\Sigma} = \int_{t-\Delta t}^{t} (M_{UCL\Sigma} \pm \Delta\varepsilon_{UCL\Sigma}) dt \tag{12}$$

where $M_{UCL\Sigma}$ is the total power demand curve for electric load, electric heating load, and electric hydrogen production load in a multi-energy grid, $\Delta\varepsilon_{UCL\Sigma}$ is the uncertainty of the total power demand of electric load, electric heating load, and electric hydrogen production load in a multi-energy network, and $X_{UCL\Sigma}$ is the total energy demand of electric load, electric heating load, and electric hydrogen production load in the multi-energy power grid.

$\Delta\varepsilon_{UCL\Sigma}$ can satisfy the following probability distribution function:

$$\begin{cases} f_{UCL,EL}(\Delta\varepsilon_{UCL,EL}) = \frac{1}{\sqrt{2\pi}\sigma_{UCL,EL}} \exp\left(-\dfrac{\Delta\varepsilon_{UCL,EL}^{2}}{2\sigma_{UCL,EL}}\right) \\ f_{UCL,HE}(\Delta\varepsilon_{UCL,HE}) = \frac{1}{\sqrt{2\pi}\sigma_{UCL,HE}} \exp\left(-\dfrac{\Delta\varepsilon_{UCL,HE}^{2}}{2\sigma_{UCL,HE}}\right) \\ f_{UCL,H2}(\Delta\varepsilon_{UCL,H2}) = \frac{1}{\sqrt{2\pi}\sigma_{UCL,H2}} \exp\left(-\dfrac{\Delta\varepsilon_{UCL,H2}^{2}}{2\sigma_{UCL,H2}}\right) \end{cases} \tag{13}$$

where $\Delta\varepsilon_{UCL,EL}$, $\Delta\varepsilon_{UCL,HE}$, and $\Delta\varepsilon_{UCL,H2}$ represent the uncertainties of electric load, electric heating load and electric hydrogen production load in actual operation, respectively, and $\sigma_{UCL,EL}$, $\sigma_{UCL,HE}$, and $\sigma_{UCL,H2}$ represent the maximum uncertainties of electric load, electric heating load, and electric hydrogen production load that may occur in actual operation, respectively.

2.4. Multi-Energy Storage Uncertainty Model

When considering the uncertainty of energy dissipation characteristics, as well as the uncertainty of energy storage and release in the charging and releasing process, within a given time Δt, the charge states of heat storage, electricity storage, and hydrogen storage facilities can be expressed as follows:

$$\begin{cases} V_{HES}(t) = C_{HERE}V_{HES}(t-\Delta t) + \Delta SOC_{HES} \\ \qquad + K_{HECR}\int_{t-\Delta t}^{t} C_{HECR}P_{HECR}(t)dt \\ V_{ELS}(t) = C_{ELRE}V_{ELS}(t-\Delta t) + \Delta SOC_{ELS} \\ \qquad + K_{ELCR}\int_{t-\Delta t}^{t} C_{ELCR}P_{ELCR}(t)dt \\ V_{H2S}(t) = C_{H2RE}V_{H2S}(t-\Delta t) + \Delta SOC_{H2S} \\ \qquad + K_{H2CR}\int_{t-\Delta t}^{t} C_{H2CR}P_{H2CR}(t)dt \end{cases} \tag{14}$$

where $V_{HES}(t)$, $V_{HLS}(t)$, and $V_{H2S}(t)$ represent the charge states of heat storage, electricity storage, and hydrogen storage facilities at time t, respectively, C_{HERE}, C_{ELRE}, and C_{H2RE} represent the energy dissipation coefficients of heat, electricity, and hydrogen storage facilities, respectively, ΔSOC_{HES}, ΔSOC_{ELS}, and ΔSOC_{H2S} represent the uncertainties of the charge states of heat storage, electricity storage, and hydrogen storage facilities corresponding to time t, respectively, C_{HECR}, C_{ELCR}, and C_{H2CR} represent the energy conversion efficiencies of heat storage, electricity storage, and hydrogen storage facilities within time intervals Δt, respectively, and K_{HECR}, K_{ELCR}, and K_{H2CR} represent the state variables of heat, electricity, and hydrogen storage facilities within time intervals Δt, respectively. When K_{HECR}, K_{ELCR}, and K_{H2CR} are equal to +1, heat storage, electricity storage, and hydrogen storage facilities operate in a charged state. When K_{HECR}, K_{ELCR}, and K_{H2CR} are equal to -1, heat storage, electricity storage, and hydrogen storage facilities operate in a state of discharge. P_{HECR}, P_{ELCR}, and P_{H2CR} represent the charging and discharging powers of heat, electricity, and hydrogen storage facilities, respectively.

In the above equation, the probability distribution of actual charge state deviations ΔSOC_{HES}, ΔSOC_{ELS}, and ΔSOC_{H2S} of electric, thermal, and hydrogen energy storage facilities, respectively, in the multi-energy power system can be described thus:

$$\begin{cases} f_{\triangle SOC_{HES}}(\Delta SOC_{HES}) = \frac{1}{\sqrt{2\pi}\sigma_{HES}} \exp\left(-\dfrac{\Delta SOC_{HES}^2}{2\sigma_{HES}}\right) \\ f_{\triangle SOC_{ELS}}(\Delta SOC_{ELS}) = \frac{1}{\sqrt{2\pi}\sigma_{ELS}} \exp\left(-\dfrac{\Delta SOC_{ELS}^2}{2\sigma_{ELS}}\right) \\ f_{\triangle SOC_{H2S}}(\Delta SOC_{H2S}) = \frac{1}{\sqrt{2\pi}\sigma_{H2S}} \exp\left(-\dfrac{\Delta SOC_{H2S}^2}{2\sigma_{H2S}}\right) \end{cases} \tag{15}$$

where σ_{HES}, σ_{ELS}, and σ_{H2S} represent the maximum uncertainties of the charge states of heat storage, electricity storage, and hydrogen storage facilities in multi-energy power system at time t, respectively.

3. Multi-Node Multi-Energy Correlation Measure with Higher-Order Markov Random Field Model (MMCM-HMRF)

In order to achieve partitioned energy coordination in multi-energy grids, this section studies the description method of heterogeneous energy balance in multi-energy grids and proposes a multivariate multi-energy flow intensity measurement method based on the Multi-energy Correlation Measure (MCM) feature index.

Then, the MMCM-HMRF model based on the Markov Random Field (MRF) [22] is established. This model can achieve the quantitative description of the multivariate topological structure relationship between adjacent nodes in multi-energy power systems, reflecting the energy balance characteristics.

3.1. Multi-Energy Correlation Measure Model (MCM)

The set of state variables for multi-energy injection or consumption at nodes in a multi-energy power system can be described thus:

$$X_{ws} = \{x_1, x_2, x_i, \ldots, x_{N-1}, x_N\} \tag{16}$$

where x_i represent the electricity, heat, and hydrogen energy injection values or consumption value of node i in the multi-energy power system and N is the total number of nodes in the multi-energy power system.

Suppose $x_p, x_q \in X_{ws}$ represent the state variables of multi-energy energy interaction between any two adjacent nodes in the network. The more energy interaction there is between two adjacent nodes $p, q(p, q \in N)$ and $s(s \in N)$, the stronger the multi-energy energy correlation between nodes p, q and s will be. The multi-energy energy balance correlation between two adjacent nodes p, q can be defined as shown below:

$$MCM_{pq} = \frac{NPQ_{pq} + \sum\limits_{i=1}^{N} NPQ_{pi}NPQ_{qi}}{1 - NPQ_{pq} + \min\left\{\sum\limits_{i=1}^{N} NPQ_{pi}, \sum\limits_{i=1}^{N} NPQ_{qi}\right\}} \tag{17}$$

where NPQ_{pq} represents the Euclidean distance between the two adjacent nodes p, q of the multi-energy power system network and the multi-energy energy injection or consumption state variable x_p, x_q, $0 \leq MCM_{pq} \leq 1$.

The MCM index matrix $MCM(X_{ws})$ of X_{ws} is depicted below:

$$MCM(X_{ws}) = \begin{bmatrix} MCM_{11} & MCM_{12} & \cdots & MCM_{1N} \\ MCM_{21} & MCM_{22} & \cdots & MCM_{2N} \\ \vdots & \vdots & \ddots & \vdots \\ MCM_{N1} & MCM_{N2} & \cdots & MCM_{NN} \end{bmatrix} \tag{18}$$

$MCM(X_{ws})$ is a symmetric and non-negative energy balance correlation matrix. This matrix transforms the correlation degree matrix of the energy balance relationship between adjacent nodes in a multi-energy power system network into a multi-variable high-order multi-energy energy state variable MCM matrix. Based on the MCM index of the multi-energy energy state variable, a high-order multi-energy energy balance correlation constraint of the energy balance relationship between adjacent nodes in the network is established, so as to introduce the high-order topological spatial correlation of the energy balance relationship between adjacent nodes in the multi-energy power system network, which in turn will achieve a better expression of the local spatial characteristics of multi-energy state variables.

3.2. MMCM-HMRF Model Based on MRF

In order to measure the multi-energy balance correlation of adjacent nodes in a multi-energy power system, firstly, the Euclidean Distance $d(x_p, x_q)$ between nodes p and q is calculated, and the energy balance correlation between adjacent nodes is normalized, so that $0 \le d_{pq} \le 1$. The normalization function is as follows:

$$d(x_p, x_q) = \exp\left\{ -\left(\|x_p - x_q\|_2\right)^2 / \left(\rho \max_{r \in N} \|x_p - x_q\|_2\right)^2 \right\} \tag{19}$$

where $\|x_p - x_q\|_2$ represents the Euclidean distance between adjacent nodes in a multi-energy power system and $\rho \le 0.2$ is the normalized scaling parameter such that the smaller the value of ρ is, the smaller the correlation of energy balance between adjacent nodes in the multi-energy power system network will be at the same distance.

The Euclidean distance measurement vector of the local region of the multi-energy power system can be calculated thus:

$$\begin{aligned} D_{ws}(X_{ws}) = \{ & d(x_p, x_1), \ldots, d(x_p, x_q) \\ & , \ldots, d\left(x_p, x_{|p| \times |p|}\right) \} \end{aligned} \tag{20}$$

In order to convert the multi-energy energy balance correlation between adjacent nodes in a multi-energy power system network into a connection strength, $D_{ws}(X_{ws})$ is converted into an adjacency strength measurement vector, $A_{ws}(X_{ws})$, by using the power adjacency function. The power adjacency function is defined as follows:

$$a_{pq}(x_p, x_q) = |d(x_p, x_q)|^{\gamma} \tag{21}$$

where $a_{pq}(x_p, x_q)$ represents the adjacency matrix weight of p, q between adjacent nodes in a multi-energy power system network. $\gamma \ge 1$, the power adjacency parameter between adjacent nodes in a multi-energy power system network, can enhance the connection strength of adjacent nodes in a strongly correlated multi-energy power system network.

Therefore, the adjacency matrix enhances the multi-energy energy balance correlation of strongly correlated multi-energy power system nodes, and effectively maintains the continuity of expression information of adjacent nodes in the multi-energy power system network. The adjacency strength measurement vector $A_{ws}(X_{ws})$ of the local region of the multi-energy power system established with multi-energy energy balance characteristics is expressed as follows:

$$\begin{gathered} A\left(x_p, x_1\right), \ldots, a\left(x_p, x_q\right), \ldots, a_{ws}\left(X_{ws}\right) \\ = \left\{a\left(x_p, x_{|ws||ws|}\right)\right\} \end{gathered} \tag{22}$$

Let the high-order topological space prior $MCM_{ws}(x_s, x_{N_s})$ of the local region ws of the multi-energy power system be expressed thus:

$$\begin{gathered} MCM_{ws}(x_s, x_{N_s}) = MCM_{up}(x_s, x_{up}) + MCM_{down}(x_s, x_{down}) \\ + MCM_{left}\left(x_s, x_{left}\right) + MCM_{right}\left(x_s, x_{right}\right) \end{gathered} \tag{23}$$

where $MCM_{up}(\bullet)$, $MCM_{down}(\bullet)$, $MCM_{left}(\bullet)$, and $MCM_{right}(\bullet)$ represent adjacent nodes of MCM which have energy interaction in MRF.

The higher order MRF prior energy term based on $MMCM$ is defined as follows:

$$E_h(x_{ws} \mid \gamma) = \sum_{p \in N_s, q \in N_s} \left[\frac{\sum\limits_{u \neq p,q} a_{pu} a_{qu} + b_{pq}}{\min\left\{ \sum\limits_{u \neq p} a_{pu}, \sum\limits_{u \neq q} a_{qu} \right\} + 1 - b_{pq}} \right] \tag{24}$$

where $E_h(x_{ws} \mid \gamma)$ represents the prior energy of the higher-order topological structure in the local region ws and b_{pq} represents the connection strength of the nodes p and q.

4. Multi-Energy Power Grid Partition Model Based on Energy Balance Demand

On the basis of the MMCM-HMRF model established earlier, this section studies the energy balance demand characteristics of the multi-energy power grid and establishes a second-order MRF model for the equilibrium state of multi-energy regions. Then, a second-order MRF model for the equilibrium state of multi-energy regions is established, and a dynamic partitioning method for multi-energy balance demand based on the Weighted Gaussian Mixture Model (WGMM) model is proposed.

4.1. Second-Order MRF Model for Equilibrium States of Multi-Energy Regions

Before establishing the second-order MRF model for the multi-energy power grid, it is necessary to study the probability characteristics of regional energy balance states in the multi-energy power grid. This section analyzes the energy balance status of nodes in the multi-energy power grid and establishes a Weighted Gaussian Mixture Model (WGMM) that can reflect the consistency of label classification for different types of energy forms [23].

For node s in a multi-energy power grid area, the set of adjacent node state variables with energy interaction is defined as x_r, such that:

$$x_r = \{x_r \mid r \in N_s\} \tag{25}$$

The WGMM likelihood model consistent with the label classification of the node energy balance state of the multi-energy power system and different energy forms is:

$$P(X \mid Y, \theta) = \prod_{s=1}^{N_s} \left[P(x_s \mid y_s, \theta) \prod_{r \in N_s} P(x_r \mid y_r, \theta)^{\frac{w(y_r)}{w_r}} \right] \tag{26}$$

where θ represents the label classification parameter of the node's energy balance state and its different energy forms, $\theta = \{\mu_l, \sigma_l^2\}_{l \in \Lambda}$, μ_l and σ_l are the mean and variance of the distribution for the l-th label classification, $\Lambda = \{0, 1, \cdots, L\}$, L represents the total number of labels for multi-energy energy balance region division, and $w_r = \sum\limits_{r \in N_s} w(y_r)$ is the normalization function. When $w(y_r) = 1$, w_r is the number of multi-energy power system nodes in the region. $w(y_r)$ is a weight function containing spatial information.

Next, a second-order MRF model for the equilibrium state of multi-energy regions is established. In local region ws of the multi-energy power system network, label field Y_{ws} of the multi-energy energy imbalance classification is an MRF based on the multi-energy energy balance state within the region. The label field is described by the *Potts* prior model, and the second-order *Potts* prior model based on the multi-energy energy imbalance region in the multi-energy power system network is obtained as follows:

$$P(y_s \mid y_{ws}, \beta) = \exp\left\{ -\beta \sum_{s,r \in N_s} [1 - \delta(y_s, y_r)] \right\} / Z(\beta) \tag{27}$$

where $Z(\beta)$ is the normalized constant of the multi-energy energy imbalance probability, β is the multi-energy imbalance probability parameter, and $\delta(y_s, y_r)$ is a function *delta* such that:

$$\delta(y_s, y_r) = \begin{cases} 1 & y_s \neq y_r \\ 0 & y_s = y_r \end{cases} \tag{28}$$

In local region ws of the multi-energy power system, when the center energy balance label y_s is not equal to the adjacent energy balance label y_r, punishment is administered thus:

$$\beta \sum_{s,r \in Ns} [1 - \delta(y_s, y_r)] \tag{29}$$

The penalty value is 0 only if y_s and y_r are equal. Therefore, the second-order *Potts* prior energy model for the multi-energy unbalanced region in the multi-energy power grid is as follows:

$$E_s(y_s, y_{ws}) = \lg P(y_s \mid y_{ws}) = \begin{cases} \beta \sum\limits_{s,r \in N_s} [1 - \delta(y_s, y_r)], y_s \neq y_r \\ 0, y_s = y_r \end{cases} \tag{30}$$

As can be seen from the above equation, in local region ws of the multi-energy power system network, when labels of more network nodes in the region tend to be consistent, the penalty value tends to 0. For the local area of the multi-energy power system with different kinds of tags, the inconsistency penalty value increases with an increase in the number of inconsistent values of nodes or expected tags of energy imbalance. This kind of regional category consistency constraint can effectively improve the edge effect of the multi-energy energy balance region division results, and it is robust to the interference of the multi-energy energy balance characteristic noise or texture signal.

4.2. Dynamic Partitioning Solution for Multi-Energy Power Grid Based on Energy Balance Demand

Based on the established WGMM model and the second-order MRF model of the multi-energy region equilibrium state, the network can be divided into regions according to the energy balance requirements. A power grid division model is established as follows:

$$\begin{aligned} F_G(Y \mid X, \Theta) = F_d(X \mid Y, \theta) + F_S(Y \mid \beta) \\ + F_h(X \mid \gamma) \end{aligned} \tag{31}$$

where $F_d(X \mid Y, \theta)$ represents the likelihood energy of local area consistency in the multi-energy power grid, $F_S(Y \mid \beta)$ represents the second-order *Potts* prior energy, $F_h(X \mid \gamma)$ represents the prior energy of the higher-order topological structure, and $\Theta = (\theta, \beta, \gamma)$.

The process of dividing the power grid into regions based on energy balance requirements, which is done to solve the optimal estimated label field Y^*, can be expressed thus:

$$\begin{aligned} Y^* &= \underset{Y}{\operatorname{argmin}} F_G(Y \mid X, \Theta) \\ &= \underset{Y}{\operatorname{argmin}} [F_d(X \mid Y, \theta) + F_S(Y \mid \beta) + F_h(X \mid \gamma)] \end{aligned} \tag{32}$$

The steps for dividing the power grid into regions based on energy balance requirements are as follows:

Step 1: Input the set of state variables of nodes in the multi-energy power system X_{ws}. Given that the number of classification labels, the mean and variance of $WGMM$, and $\{\mu_l, \sigma_l^2\}_{l\in\Lambda}$ are randomly initialized, the prior parameter β is given by an experiment where $\rho = 0.2, \gamma = 4$.

Step 2: Calculate the higher-order topological structure prior energy $E_h(x_{ws} \mid \gamma)$ of the local area of the multi-energy network based on the pre-partition results of the multi-energy network region ws.

Step 3: Calculate the mean and variance of WGMM model label distribution $\{\mu_l, \sigma_l^2\}_{l\in\Lambda}$ in the local region ws.

Step 4: For each multi-energy power system node, calculate the energy allocated to the label in its local area: $E_{ws}\left(y_s \mid x_{ws}, \mu_l, \sigma_l^2, \rho, \beta, \gamma\right)$.

Step 5: Calculate the global energy $F_G^{(n)}(Y) = \sum_s E_{ws}^{(n)}(y_s)$. If $\left|F_G^{(n)}(Y) - F_G^{(n-1)}(Y)\right| \le \varepsilon$ is a small constant, then $Y^* = Y^{(n)}$ and the algorithm terminates, outputting the optimal label field $Y^* = \{y_s \mid y_s \in \Lambda, s \in N_S\}$. Otherwise, go back to Step 2 to continue the process of iteration.

5. Example Analysis

This section establishes a simulation system based on the actual operating data of the Liaoning power grid, the multi-energy power system topology structure that includes flexible adjustment resources such as new energy sources represented by wind and solar power generation, electric heat storage, electric hydrogen storage and hydrogen fuel cells, chemical battery energy storage, thermal power and hydropower, and other traditional synchronous power sources, as shown in Figure 2, there are 30 multi-energy nodes in the power grid. In Figure 2, nodes 1, 2, and 3 are new energy nodes, and nodes 3, 4, and 5 are electric heat storage nodes, electric hydrogen storage and fuel cell nodes, and chemical cell nodes, respectively. Nodes 13 and 27, 23, and 22 are thermal power, hydropower, and gas power generation nodes, respectively. It is assumed that the central control center is located at six nodes—6, 7, 8, 17, 18, and 27—with 200 electric vehicles in each area.

According to the topology structure in Figure 2, with reference to the actual power supply and load situation of the power grid, the simulation example parameters are set as shown in Tables 1 and 2. The typical new energy power output, load, and energy storage power curves of the system are shown in Figures 3 and 4, and the uncertainty curves of the power supply, load, energy storage, and electric vehicle in the system are shown in Figure 4.

Table 1. Parameter table of multi-energy power system.

Node Number	Source Type	Power Capacity (MW)	Energy Storage Type	Energy Storage Capacity (MW)
1	Wind power	600		
2	Photovoltaic power	480		
3	Wind power	500	Electric heating and heat storage facilities	620
4			Electric hydrogen production facilities and hydrogen fuel cell	32
5			Chemical battery	100
13,27	Thermal power	3650		
22	Gas power	150		
23	Hydropower	300		

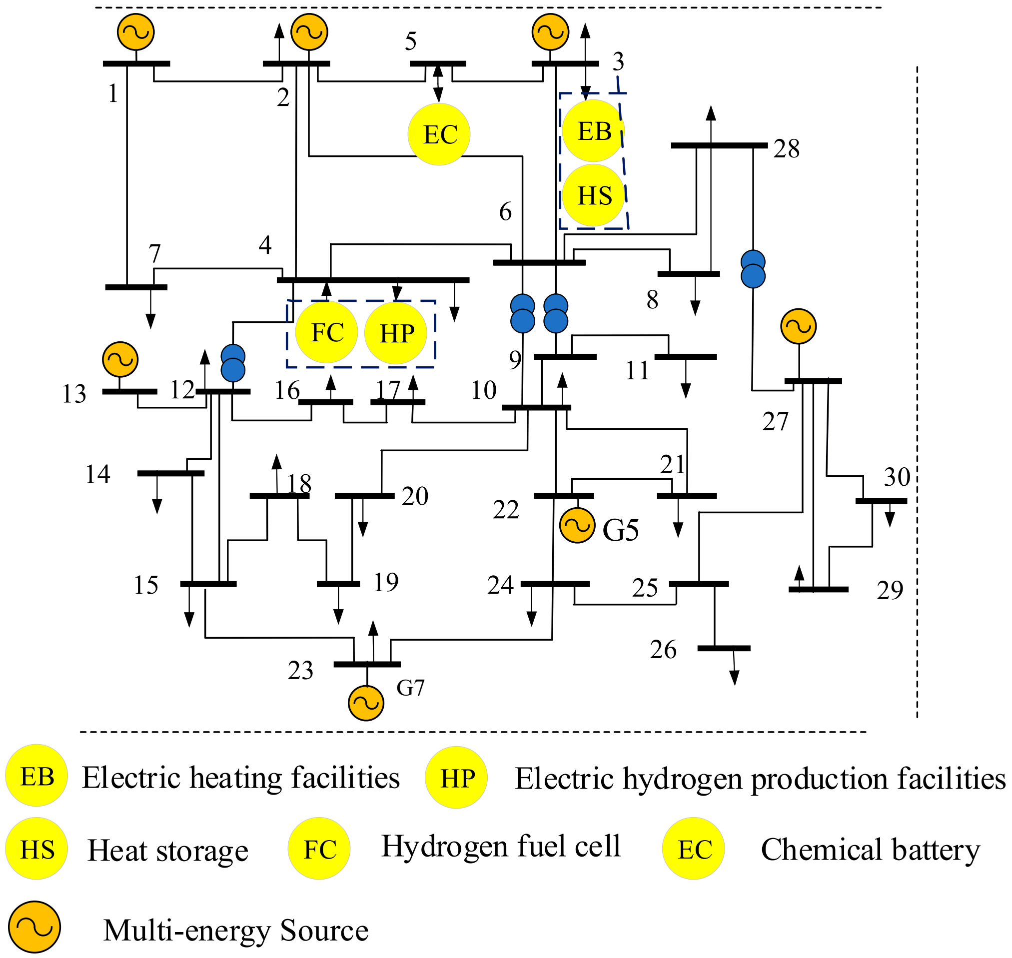

Figure 2. Topology of the new energy power system.

Table 2. Electric Vehicle Parameter Table.

Parameter Name	Data
Electric vehicle capacity	32 kw·h
Charging and discharging power	4 kw
Charging and discharging efficiency	0.9
Power consumption per 100 km	15 kw·h

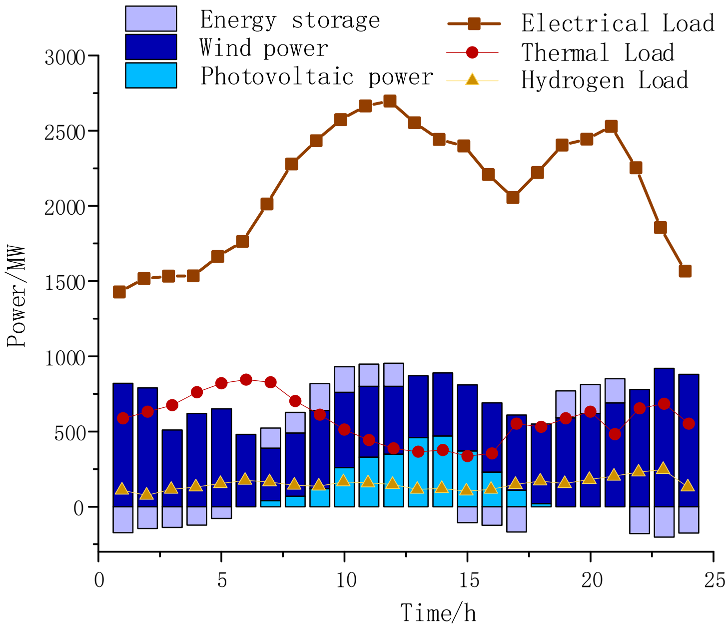

Figure 3. Typical new energy power output, load, and energy storage power curve of the system.

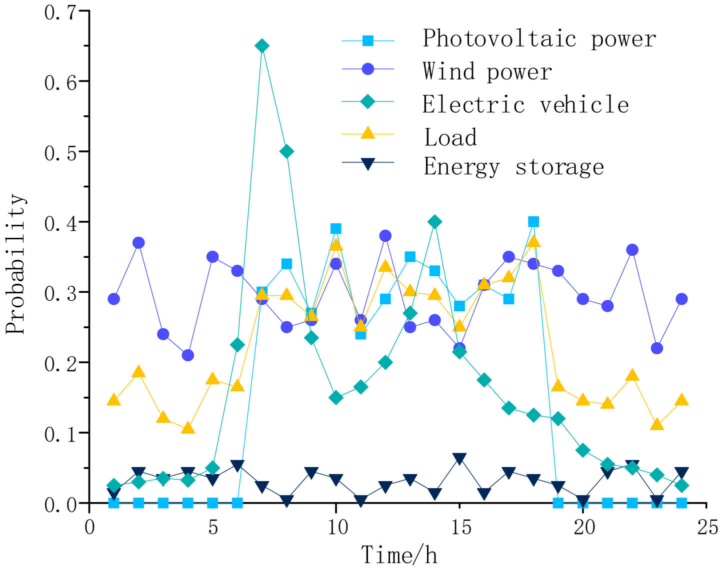

Figure 4. Uncertainty distribution curve of typical new energy power output, load, energy storage, and electric vehicle response in the system.

5.1. Simulation Analysis of Multi-Energy Power Grid Partition

The following is a simulation verification of the dynamic partitioning method for energy balance in multi-energy networks that is proposed in this article. Before solving the partitioning problem, the pre-partitioning results of the multi-energy network are shown in Figure 5.

The energy balance zoning optimization model established in this article is used to solve the zoning problem. Based on the pre-partitioning results shown in Figure 5, combined with the system source, load, and storage operating states and uncertainties shown in Figures 3 and 4, the multi-energy system is partitioned according to the energy balance adjustment requirements. The result of the multi-energy power grid partition is shown in Figure 6.

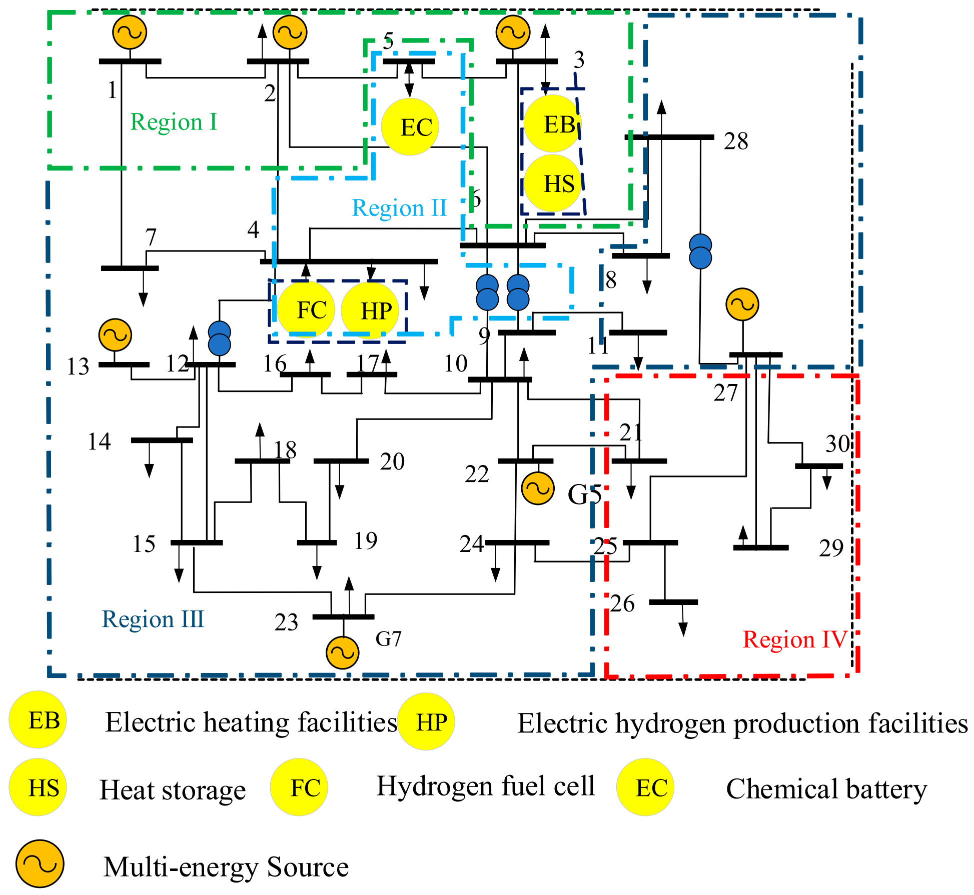

Figure 5. Pre-partition result of the multi-energy power grid.

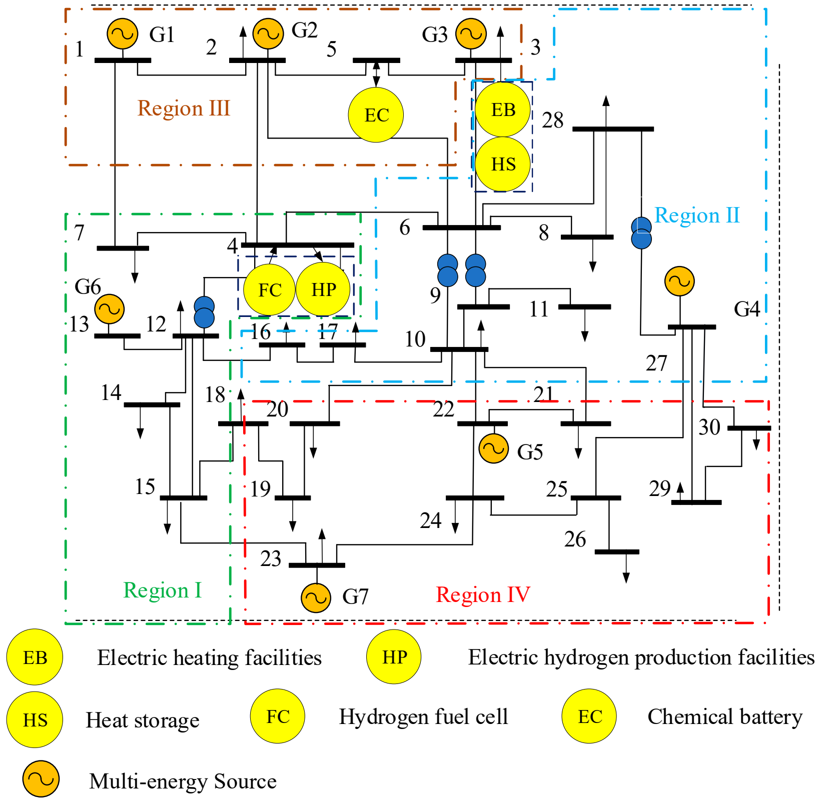

Figure 6. Partition result of the multi-energy power grid.

Due to the configuration of heat storage, electricity storage, and hydrogen storage facilities at certain nodes of a multi-energy power system, the energy balance regulation capabilities for different types of energy in different regions of the power grid are also different. The characteristic of energy balance regulation in multi-energy power systems determines that when optimizing and scheduling multi-energy flexible resource peak shaving, it is necessary to fully consider the distribution characteristics of multi-energy loads, multi-energy storage, and new energy sources in the power grid in order to effectively improve the efficiency and economy of multi-energy peak shaving.

5.2. Energy Balance Analysis of Multi-Energy Power Grid under Partitioned Operation

Based on the energy supply and demand situation, and its uncertainty characteristics in the systems shown in Figures 3 and 4 combined with the power grid pre-partitioning results shown in Figure 5, the corresponding peak shaving capacity curves of the multi-energy power grid can be obtained as shown in Figures 7–9.

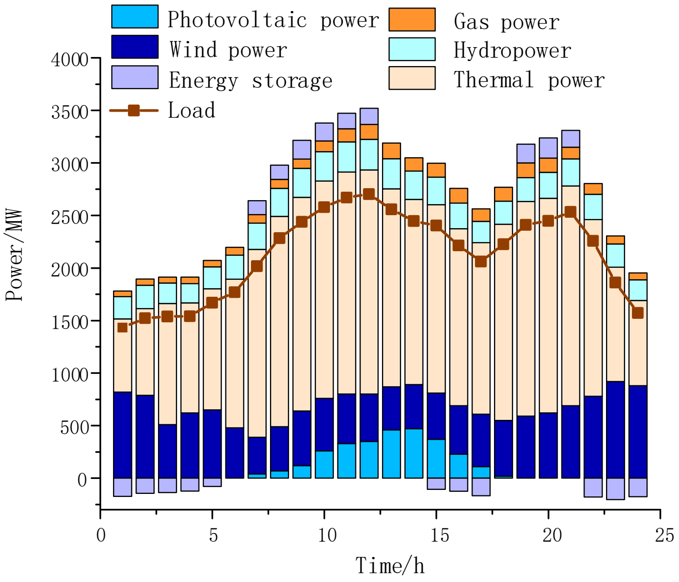

Figure 7. Peak shaving capacity allocation of electric energy.

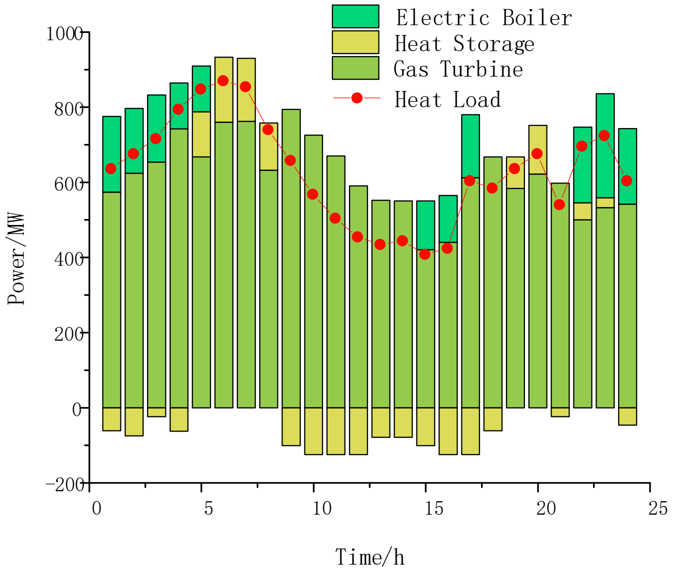

Figure 8. Peak shaving capacity allocation of thermal energy.

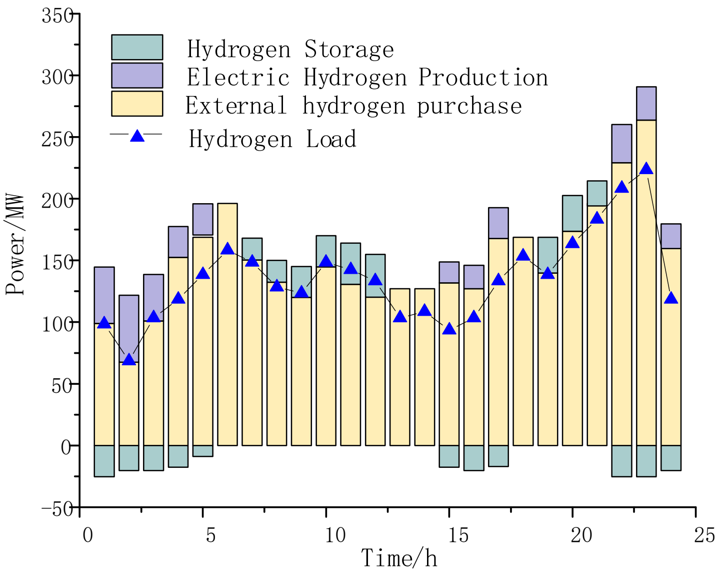

Figure 9. Peak shaving capacity allocation of hydrogen energy.

From Figures 7–9, it can be seen that in order to ensure a high level of power balance in a multi-energy power grid under high uncertainties, it is necessary to configure more flexible resource adjustment units when scheduling plans. At the same time, the reserved adjustment capacity of each flexible resource adjustment unit is also relatively large. At this point, in order to cope with a higher proportion of new energy and with uncertainty, the total adjustment cost of the power grid is high. The large proportion of traditional energy supply methods also brings significant pressure to the improvement of the system's carbon reduction capacity.

Based on the energy balance partitioning results of the multi-energy power grid shown in Figure 6, the allocation of flexible resource peak shaving capacity in the network after partitioning optimization is shown in Figures 10–12.

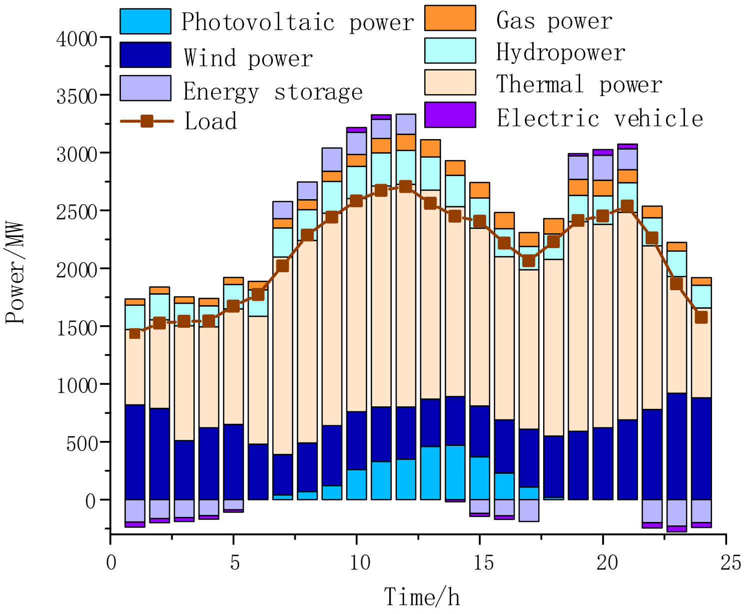

Figure 10. Peak shaving capacity allocation of electric energy after power grid partitioning.

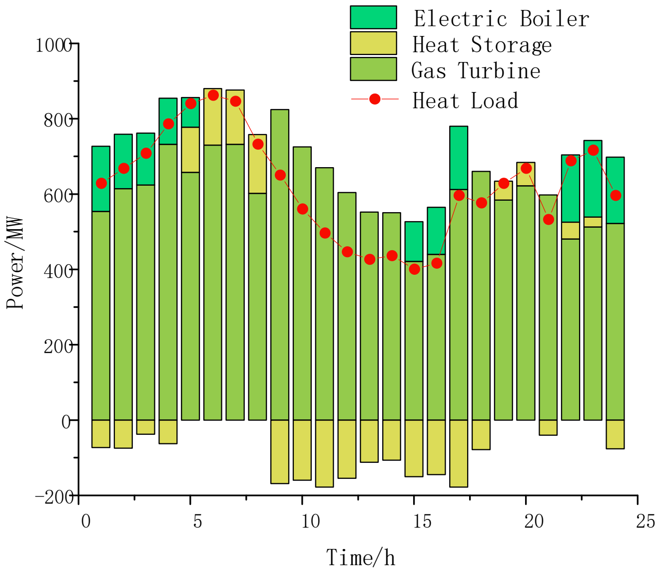

Figure 11. Peak shaving capacity allocation of thermal energy after power grid partitioning.

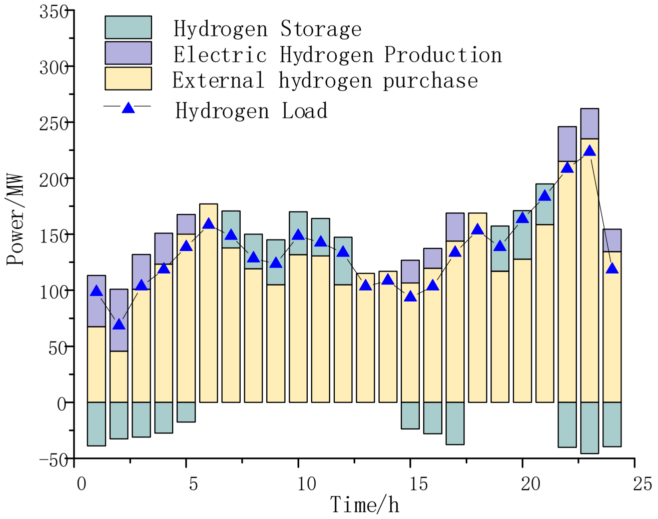

Figure 12. Peak shaving capacity allocation of hydrogen energy after power grid partitioning.

From Figures 10–12, it can be seen that the adjustment depth of the multi-energy conversion device in the optimized network significantly increases throughout the day. The peak shaving reserve capacity of various energy sources decreases by varying degrees throughout all energy supply periods. Overall, the proportion of capacity allocation for traditional energy supply units in these figures has decreased.

Therefore, allocating the peak shaving capacity of a multi-energy power grid based on the optimized partitioning results can effectively coordinate the complementary characteristics of multi-energy regulation resources in different regions or nodes of the system. Furthermore, the regulatory potential of energy conversion equipment is fully utilized in such a scenario, effectively reducing the proportion of traditional energy supply methods and peak shaving capacity and improving the utilization rate of renewable energy. Moreover, after partition optimization, the system can coordinate and dispatch multiple energy sources and storages across the entire network based on the different types of energy regulation characteristics in different regions, effectively reducing the overall peak shaving demand of the entire network.

6. Conclusions

This article proposes a dynamic partitioning model for energy balance in multi-energy power grids that considers the willingness of electric vehicles to respond, and the uncertainties of source, load and storage, to address the significant differences in power and energy balance at different time and spatial scales in multi-energy power grids.

This model is based on a prior model of higher-order topology structure for multi-energy interaction, and can divide the network into regions according to the energy balance requirements of the multi-energy network in consideration. To verify the effectiveness of this model, this paper constructed a simulation model based on actual operating power grid data. The simulation results indicate that:

(1) The energy balance zoning method proposed in this article can fully consider the uncertainties of source, load, and storage in the network and quickly and accurately identify local areas of the multi-energy grid where energy imbalance exists. Furthermore, it can optimize the partitioning of multi-energy networks to achieve the peak shaving optimization of different energy forms and maximize energy utilization.
(2) After partitioning the multi-energy power grid based on the energy balance requirements, the complementary coordination ability between multiple types of energy equipment in the multi-energy network can be fully utilized, effectively reducing the startup mode and peak shaving capacity of traditional energy supply units and improving the utilization rate of renewable energy.
(3) After optimizing the demand for multi-energy balance regulation, the system can coordinate and dispatch the load and storage of multiple energy sources in the entire network based on the different types of energy regulation characteristics in different regions, effectively reducing the total peak shaving demand of the entire network and thus achieving the efficient and stable operation of the multi-energy grid.

Author Contributions: This article was written by S.Q., who carried out the design and data analysis of the main research. K.Z. led the writing of the article, Z.C. (Zhuo Chen) and Y.M. proofread all the drafts, and Z.C. (Zhe Chen) gave guidance to the paper. All authors have made contributions to the writing and revision of the article, and have made suggestions for improvement to ensure that the article can accurately express complex research results. All authors have read and agreed to the published version of the manuscript.

Funding: This research was funded by the National Key Research and Development Program of China (No. 2017YFB0902100).

Data Availability Statement: The simulation analysis part of this article is based on real operating power grid data, and for confidentiality reasons, the data in this article will not be disclosed.

Conflicts of Interest: The authors declare no conflict of interest.

References

1. Wang, R.; Ma, D.; Li, M.-J.; Sun, Q.; Zhang, H.; Wang, P. Accurate Current Sharing and Voltage Regulation in Hybrid Wind/Solar Systems: An Adaptive Dynamic Programming Approach. *IEEE Trans. Consum. Electron.* **2022**, *68*, 261–272. [CrossRef]
2. Rui, W.; Qiuye, S.; Dazhong, M.; Xuguang, H. Line Impedance Cooperative Stability Region Identification Method for Grid-Tied Inverters Under Weak Grids. *IEEE Trans. Smart Grid* **2020**, *11*, 2856–2866. [CrossRef]
3. Cesena, E.A.M.; Mancarella, P. Energy Systems Integration in Smart Districts: Robust Optimisation of Multi-Energy Flows in Integrated Electricity, Heat and Gas Networks. *IEEE Trans. Smart Grid* **2019**, *10*, 1122–1131. [CrossRef]
4. Rui, W.; Qiuye, S.; Pinjia, Z.; Yonghao, G.; Dehao, Q.; Peng, W. Reduced-Order Transfer Function Model of the Droop-Controlled Inverter via Jordan Continued-Fraction Expansion. *IEEE Trans. Energy Convers.* **2020**, *35*, 1585–1595. [CrossRef]
5. Huang, W.; Zhang, N.; Yang, J.; Wang, Y.; Kang, C. Optimal Configuration Planning of Multi-Energy Systems Considering Distributed Renewable Energy. *IEEE Trans. Smart Grid* **2019**, *10*, 1452–1464. [CrossRef]
6. Yunshou, M.; Jiekang, W.; Ruidong, W.; Zhihong, C.; Ran, Z.; Lingmin, C.; Wenjie, Z. A Collaborative Demand-Controlled Operation Strategy for a Multi-Energy System. *IEEE Access* **2021**, *9*, 80571–80581. [CrossRef]
7. Damavandi, M.Y.; Bahramara, S.; Moghaddam, M.P.; Haghifam, M.-R.; Shafie-Khah, M.; Catalao, J.P.S. Bi-level approach for modeling multi-energy players' behavior in a multi-energy system. In Proceedings of the 2015 IEEE Eindhoven PowerTech, Eindhoven, The Netherlands, 29 June–2 July 2015; pp. 1–6. [CrossRef]

8. Bschorer, S.; Kuschke, M.; Strunz, K. Object-oriented modeling for planning and control of multi-energy systems. *CSEE J. Power Energy Syst.* **2019**, *5*, 355–364.
9. Yan, N.; Zhong, Y.; Li, X.; Wang, Y.; Su, L.; Jiang, W.; Zhou, J. Energy Management Method of Electricity Heat Hydrogen Multi-Coupling System for Retired Power Battery Echelon Utilization in Microgrids. *IEEE Trans. Appl. Supercond.* **2021**, *31*, 0604605. [CrossRef]
10. Zhou, X.; Sang, M.; Bao, M.; Wang, S.; Cui, W.; Ye, C.; Ding, Y. Exploiting Integrated Demand Response for Operating Reserve Provision Considering Rebound Effects. *IEEE Access* **2022**, *10*, 15151–15162. [CrossRef]
11. Greening, B.; Braunholtz-Speight, T.; Wood, R.; Freer, M. Batteries and beyond: Multi-vector energy storage as a tool to decarbonise energy services. *Front. Energy Res.* **2023**, *10*, 1109997. [CrossRef]
12. Yang, H.; Li, M.; Jiang, Z.; Zhang, P. Multi-Time Scale Optimal Scheduling of Regional Integrated Energy Systems Considering Integrated Demand Response. *IEEE Access* **2020**, *8*, 5080–5090. [CrossRef]
13. Jin, H.; Teng, Y.; Zhang, T.; Wang, Z.; Deng, B. A locational Marginal Price-Based Partition Optimal Economic Dispatch Model of Multi-Energy Systems. *Front. Energy Res.* **2021**, *9*, 694983. [CrossRef]
14. López, V.; Jove, E.; Gato, F.Z.; Pinto-Santos, F.; Piñón-Pazos, A.J.; Casteleiro-Roca, J.-L.; Quintian, H.; Calvo-Rolle, J.L. Intelligent Model for Power Cells State of Charge Forecasting in EV. *Processes* **2022**, *10*, 1406. [CrossRef]
15. Wang, P.; Xu, J.; Yan, Q.; Lin, H. A two level scheduling optimization model for building microgrids considering demand response and uncertainties of flexible load resources. *Electr. Power Constr.* **2022**, *43*, 128–140.
16. Jawale, S.A.; Singh, S.K.; Singh, P.; Kolhe, M.L. Priority Wise Electric Vehicle Charging for Grid Load Minimization. *Processes* **2022**, *10*, 1898. [CrossRef]
17. Chen, X.; Jia, Y.; Tong, X.; Li, Z. Research on Pedestrian Detection and DeepSort Tracking in Front of Intelligent Vehicle Based on Deep Learning. *Sustainability* **2022**, *14*, 9281. [CrossRef]
18. Wang, R.; Sun, Q.; Hu, W.; Li, Y.; Ma, D.; Wang, P. SoC-Based Droop Coefficients Stability Region Analysis of the Battery for Stand-Alone Supply Systems with Constant Power Loads. *IEEE Trans. Power Electron.* **2021**, *36*, 7866–7879. [CrossRef]
19. Cao, Y.; Wang, T.; Kaiwartya, O.; Min, G.; Ahmad, N.; Abdullah, A.H. An EV Charging Management System Concerning Drivers' Trip Duration and Mobility Uncertainty. *IEEE Trans. Syst. Man, Cybern. Syst.* **2018**, *48*, 596–607. [CrossRef]
20. Zhang, X.; Chen, Y.; Wang, Y.; Ding, R.; Zheng, Y.; Wang, Y.; Zha, X.; Cheng, X. Reactive Voltage Partitioning Method for the Power Grid With Comprehensive Consideration of Wind Power Fluctuation and Uncertainty. *IEEE Access* **2020**, *8*, 124514–124525. [CrossRef]
21. Alanazi, M.S. A Modified Teaching—Learning-Based Optimization for Dynamic Economic Load Dispatch Considering Both Wind Power and Load Demand Uncertainties With Operational Constraints. *IEEE Access* **2021**, *9*, 101665–101680. [CrossRef]
22. Descombes, X.; Morris, R.; Zerubia, J.; Berthod, M. Estimation of Markov random field prior parameters using Markov chain Monte Carlo maximum likelihood. *IEEE Trans. Image Process.* **1999**, *8*, 954–963. [CrossRef] [PubMed]
23. Bahari, M.H.; Dehak, N.; Van Hamme, H.; Burget, L.; Ali, A.M.; Glass, J. Non-Negative Factor Analysis of Gaussian Mixture Model Weight Adaptation for Language and Dialect Recognition. *IEEE/ACM Trans. Audio, Speech, Lang. Process.* **2014**, *22*, 1117–1129. [CrossRef]